J. Fluid Mech. (1986), *vol.* 173, *pp.* 95–114
Printed in Great Britain

Bubble formation, motion and interaction in a Hele-Shaw cell

By T. MAXWORTHY

Departments of Mechanical and Aerospace Engineering, University of Southern California, Los Angeles, CA 90089-1453, USA

(Received 4 March 1986)

We consider the motion of the flattened bubbles which form when air is injected into a viscous fluid contained in the narrow gap between two flat, parallel plates which make up a conventional Hele-Shaw cell, inclined at an angle α to the horizontal. We present a number of qualitative observations on the formation and interaction of the streams of bubbles that appear when air is injected continuously into the cell. The majority of this paper is then concerned with the shape and velocity of rise of single, isolated bubbles over a wide range of bubble size and cell inclination. We compare these results to theories by Taylor & Saffman (1959), and Tanveer (1986). It appears that the bubble characteristics found by an *ad hoc* speculation in Taylor & Saffman (1959) and by Tanveer (1986) only agree with the experimental results in the limit $\alpha \to 0$, and for large bubble widths (D). For finite values of α, it is necessary to use the measured bubble shape in order to calculate the rise velocity using the more general Taylor & Saffman (1959) formulation. Deviations from these theories for small D can be explained by considering the effects of the detailed flow close to the bubble surface.

1. Introduction

While the problem of the motion of individual spherical or oblate bubbles in an extended viscous fluid medium has had a very long history (see Levich 1962; Happel & Brenner 1973 for example) the corresponding motion of bubbles between the two, closely spaced, constraining, parallel walls of a Hele-Shaw cell, has not, as far as we are aware, with the only relevant papers being Taylor & Saffman (1959, hereinafter referred to as TS) and Tanveer (1986).† This geometry has been the centre of much attention recently and the present paper describes more of the fascinating array of phenomena which can be produced in such a simple device. Up to the present, there has been extensive experimentation and calculation of the linear instability and nonlinear growth of an initially flat interface to a single, large finger in the case where instability is produced by fluid injection into a horizontal Hele-Shaw cell, by Saffman & Taylor (1958), Park & Homsy (1984), Tryggvason & Aref (1983) among many, and by Maxworthy (1987) when the instability is driven by a gravitational potential in the absence of fluid injection. During the latter experiments we noted that at the late stages of the nonlinear motion of an initially flat interface large, individual bubbles were generated but their characteristics could not be predicted nor controlled. In a series of follow-on experiments, to study the instability of an interface under the combined action of both continuous fluid (air) injection and gravity, we noted, that

† I am indebted to the referees of the first version of this paper for pointing out these references to me.

at low injection rates, the structures that were formed rose under the action of gravity and became detached from their air supply to continue rising as individual bubbles. In this way a train or stream of bubbles could form and these had such fascinating interaction properties that we are devoting considerable effort to their study. A preliminary report of these effects is reported here with greater detail to be presented in a future publication. In order to understand the dynamics of these bubble-streams it was first necessary to characterize the motion of the individual bubbles, these studies are presented in detail here.

Bubbles rising in such a constricted geometry are of interest in the geophysics of oil recovery where oil-bearing strata are deliberately cracked by secondary injection at very high pressures, and in geothermal systems where one might suppose that there are circumstances where they have to rise in a medium made up of a number of interconnected cracks filled with a more viscous fluid. One can also imagine possible applications in bio-engineering, e.g. in blood-oxygenation, heart–lung replacement machines and in other direct-contact mass and heat transfer devices in technological applications.

From a dynamical point of view they are of some interest because one can study large Reynolds number ($Re = UD/\nu$) flows, based on bubble width (D) velocity (U) and fluid kinematic viscosity, ν, using methods which are still basically linear. The latter property of Hele-Shaw flows is already well known since it is the parameter $Re\,(h/D)^2$ which is important (Riegels 1938). Here h is the width of the gap between the plates which make up the main structure of the cell. Typically Re can be $O(10^3)$ before the control parameter, $Re\,(h/D)^2$ approaches unity. This approach is used in the preliminary theoretical section, §4. In §2 we discuss the apparatus and experimental procedures and in §3 the preliminary observations of the interactions between the members of a rising stream of bubbles. The basic theories of TS and Tanveer (1986) together with some alternative derivations for the motion of single bubbles are given in §4. In §§5 and 6 we present the experimental results and a comparison with the basic theory of §4 together with a discussion and extended theoretical arguments to explain why the basic theory applies in only a limited parameter range.

2. Apparatus and procedure

The basic Hele-Shaw cell is shown in figure 1. It consisted of two 30×90 cm $\times \frac{3}{4}''$ thick Lucite sheets bolted together with a $\frac{1}{16}''$ spacer between them so that the gap width h was 0.180 cm, when the effect of a thin layer of sealing compound was taken into account. Various filling and emptying holes and air injection devices were attached to the upper plate. The cell was filled with a viscous silicone oil and was supported in a metal frame at various angles α to the horizontal. Air could either be injected continuously through the central hole at the bottom of the cell (figure 1) to study bubble streams or in controlled finite amounts to observe the motion of single bubbles. In the first case the interactions were recorded photographically at fixed intervals of time, while in the second the velocity of rise, U, of a given bubble was found by timing its passage between two marks on the upper plate while the bubble shape and dimension were measured from a photographic image of the bubble. The viscosity ν and surface tension σ of the oil were found using standard methods so that, at the operating temperature of the cell (21 °C), $\nu = 0.778$ cm^2/s and $\sigma = 21.0$ dynes/cm.

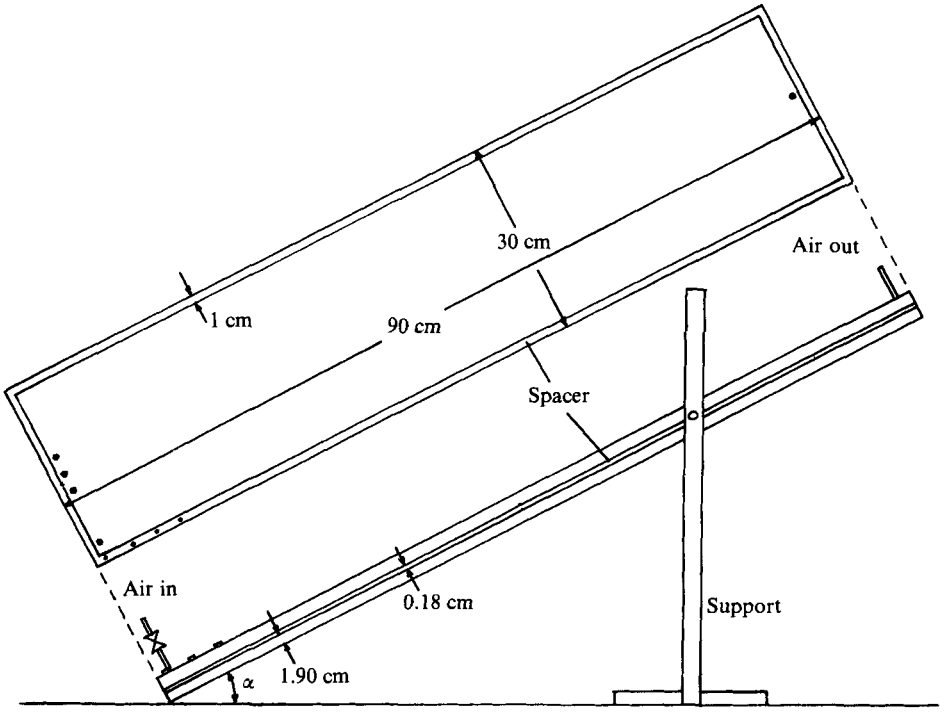

FIGURE 1. Apparatus.

3. Continuous air injection: the formation and interaction of bubble streams†

When air was continuously injected into the inclined cell at the lower central hole a bubble began to form and grow. As it did so, it rose under the action of the buoyancy force acting upon it, and eventually became disconnected from its supply of air to continue rising as a self-contained entity. Since the air supply was constant, another bubble began to form in its place, to rise and to become disconnected. In this way a stream or train of bubbles of apparently equal size and spacing was formed. If the spacing was small enough, typically less than about 3–4 bubble diameters in our particular cell, alternate bubbles would catch up with their upstream neighbours to form a bubble pair. Under certain circumstances these bubble duos would pair again to form a stack of four bubbles. Further pairing created eight-bubble stacks, etc. an example of this process is shown in figure 2 (*a*). The locations and times at which these pairings took place were not constant, apparently depending on imperceptible variations in the initial bubble sizes and spacings. This spatial and temporal jitter or chaos is very reminiscent of similar behaviour in the other nonlinear, dynamical fluid systems, e.g. the 'dripping faucet' (Shaw 1984), vortex pairing in a plane shear layer, etc. and may serve as a simple alternative to, or model of such systems, a hypothesis we intend to explore in depth in the future.

Fortunately, the relatively straightforward behaviour described above was only

† This section was added at the suggestion of a referee of the first version of this paper. Despite its present lack of quantitative results, the observations do give some idea of the wide variety of forms which such a simple system can generate and point to further experiments in which the quantitative aspects of the phenomena can be examined in depth.

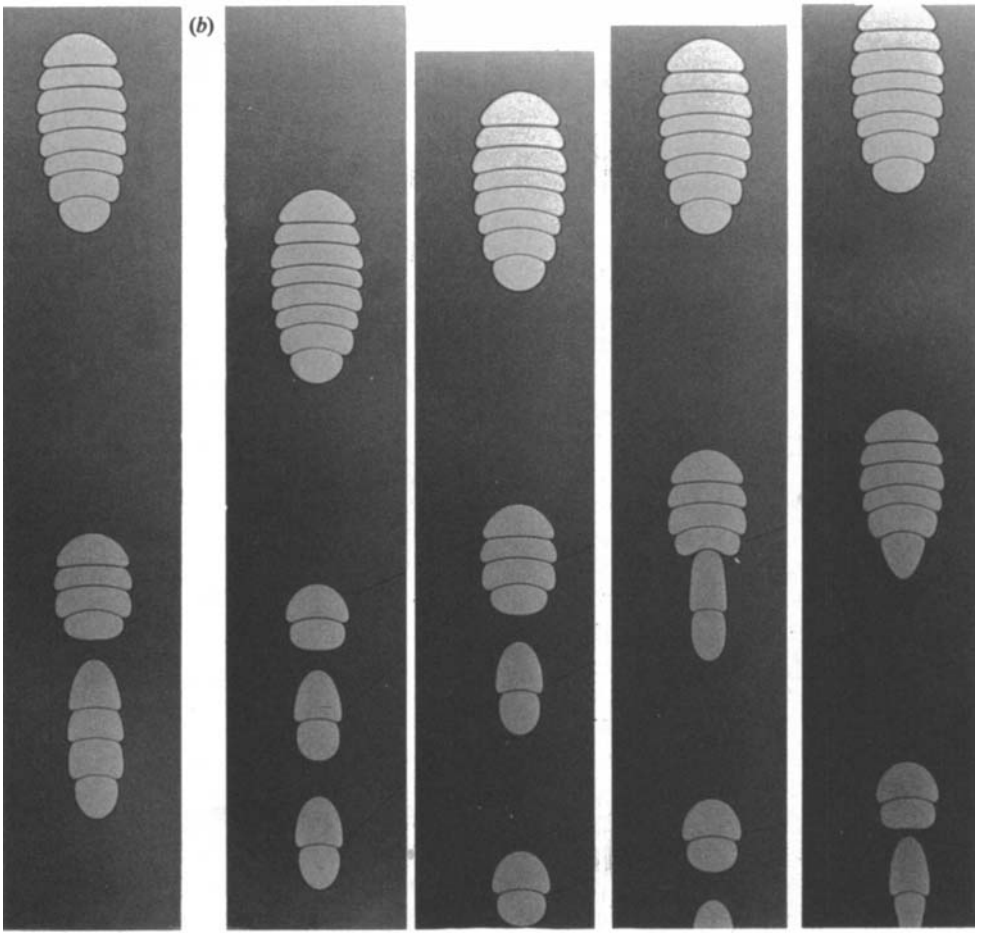

FIGURE 2. The individual bubbles, formed at the bottom of the cell, pair to produce bubble duos, initially these undergo further pairings to produce stacks of eight bubbles (first vertical strip (*a*)). The bubble stack below the eight-bubble stack in the next sequence of strips (*b*) has six members only, indicating the occasional breaking of the uniformity of the pairing process.

one of a bewildering variety of responses which could be generated. For example, under some circumstances the bubble stacks would undergo a 'tip-splitting' instability and form two trains of bubbles rising side-by-side (figure 3*a*). Often the thin 'membranes' separating the individual members of a stack would rupture while others would become unstable, to generate segmented stacks of surprising beauty (figures 3*b–d*). Often one particular pattern would repeat itself many times, to be suddenly replaced by a different pattern which would in turn persist for a long time before being replaced by either the original pattern or sometimes a new one. The length of time each pattern existed was variable, itself exhibiting a chaotic behaviour.

Other interesting observations have been made, but probably none was more fascinating than that which occurred when a very small bubble, typically of a diameter of the order of the cell gap width, became attached to the nose of a much larger single bubble or bubble stack. The bubble velocity and ellipticity increased dramatically, by factors of between 2 and 10 depending on the relative sizes of the bubbles. We attribute this to the subtle change in the boundary conditions at the

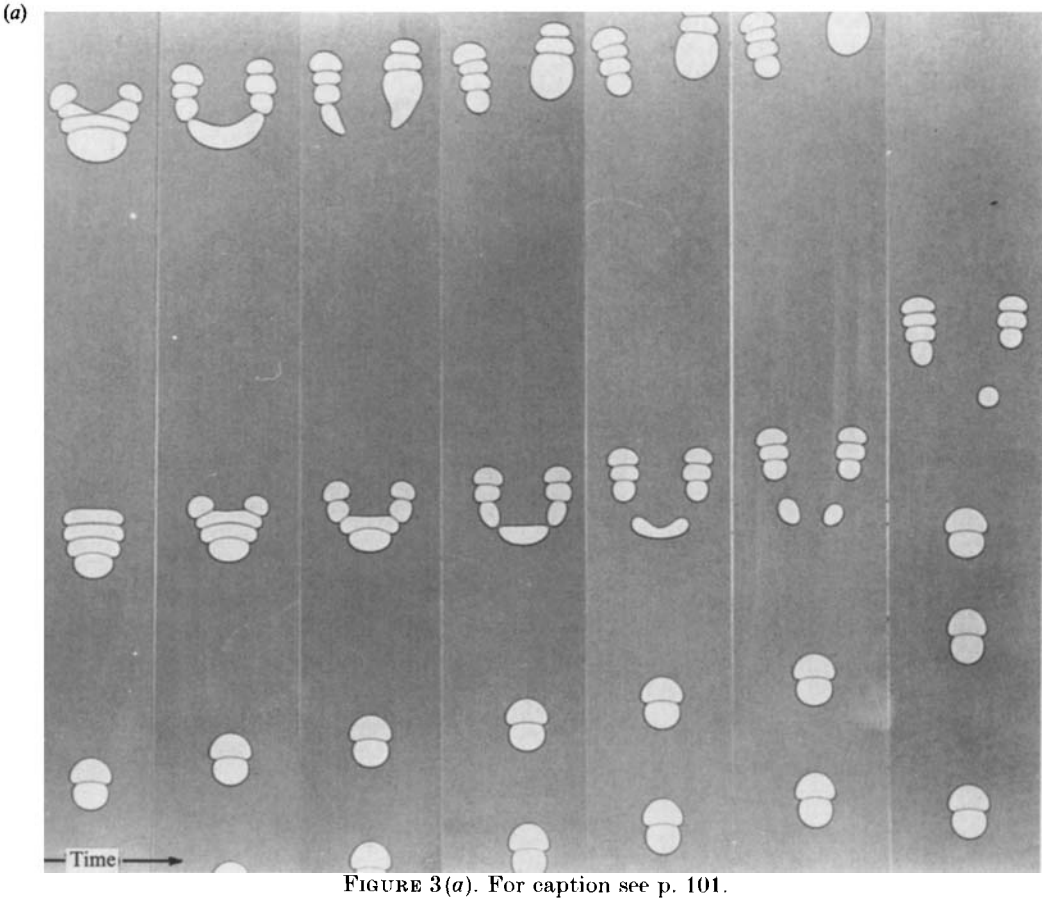

FIGURE 3(*a*). For caption see p. 101.

bubble nose that such a small bubble must induce. We sketch the details in figure 4(*a*). The observations suggest that the curvatures of the interfaces which meet as shown in figure 4(*a* i) are determined by a balance between surface-tension forces and gravity, with viscous forces playing a minor role (see footnote to §4.1), since a static interface (figure 4*a* ii) has the same shape in the immediate vicinity of the intersection (figure 4*a* iii). Thus the initial curvature and slope of the bigger bubble become much larger at the tip, than originally, and set the initial boundary shape from which the lower part of the bubble evolves to a much more slender form (figure 4*b*).

The theories to be presented in the next section show that, not surprisingly, such slender bubbles rise faster than fatter ones of the same area, thus this observation provides an example of a flow where an apparently insignificant defect has a major effect. The existence of a small bubble on a very much larger bubble can also induce a beautiful symmetric wavelike instability (figure 4*c*). It appears that this instability is virtually identical with that reported by Couder *et al.* (1986) for the case of a small bubble attached to the tip of the long 'finger' produced by continuous air injection into a horizontal cell, except for the subtle and probably minor secondary effects of gravity. A larger tip-bubble causes an oscillation of the tip and an asymmetric wave on the larger bubble (figure 4*d*).

All of the qualitative observations presented here have made it obvious that much

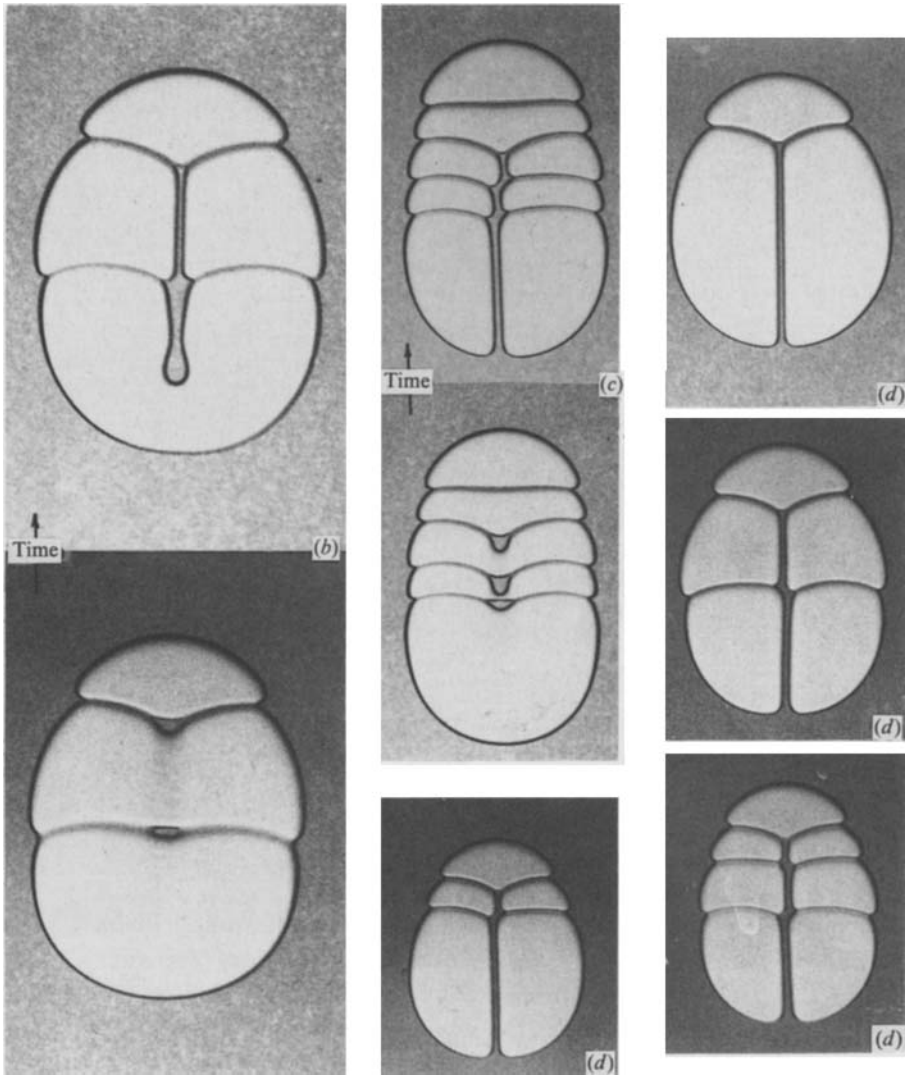

FIGURE 3(*b–d*). For caption see facing page.

more work is needed to explain everything we have seen. As a first step, in the rest of this paper, we examine the dynamics of single bubbles in considerable detail leaving more complex questions of bubble interactions and instabilities to future papers.

4. The dynamics of single bubbles

4.1. *Preliminary theoretical considerations*

The basic characteristics of the flow around a single bubble rising in a viscous fluid in a narrow gap are shown in figure 5. Here we note that the flow can be conveniently divided into at least two clear-cut regions.† In the outer region, away from the immediate influence of the details of the motion near the bubble surface, the flow is that due to a moving cylinder in a Hele-Shaw cell, i.e. the mean flow, although

† Devotees of the method of matched asymptotic expansion will be aware, immediately, of the possibility of the use of such techniques here. For our present purposes they are replaced by intuitively simpler arguments to be augmented later.

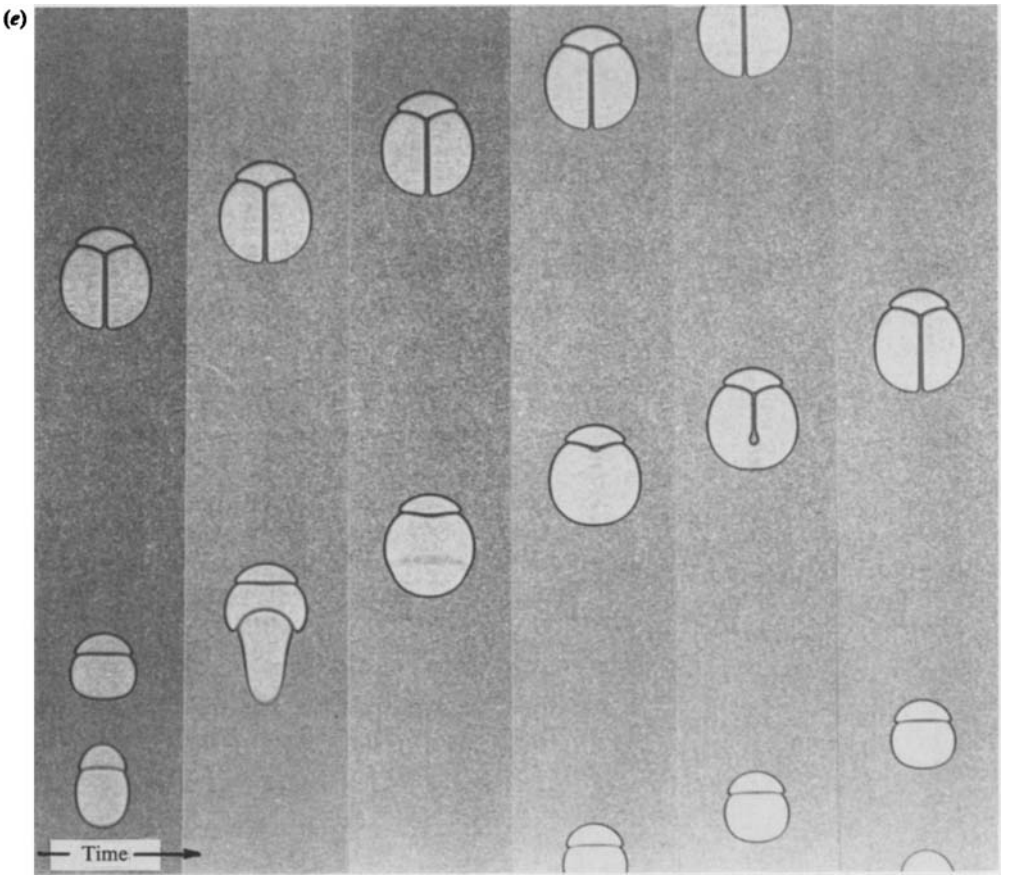

FIGURE 3 (*a*) A stack of four bubbles becomes distorted at its nose and splits into two bubble streams rising side-by-side. This bubble splitting process also occurs in single bubbles. In both cases if the splitting is not symmetric the smaller entity can become re-entrained into the rear of the larger. (*b*), (*c*), (*d*) and (*e*) Examples of membrane breaking and instability to produce vertically segmented bubbles.

viscous, obeys Laplace's equation in the plane of the gap (figure 5*a*). As will be come apparent, because the bubble does not completely fill the gap between the plates (figure 5*b*) the outer flow is actually that due to a moving porous cylinder (see §5). Close to the bubble surface, gravitational G, viscous V, inertia I and surface-tension S forces† compete to determine both the detailed shape of the interface and the enhanced dissipation in its neighbourhood (§6).

† A dimensional analysis to determine the relative importance of each of these forces reveals the known dependence on the capillary number $V/S = Ca = U\mu/\sigma$ which has been used many times previously to parameterize the conditions at the interface and which usually has a value of 0.2 or less. The Reynolds number $I/V = Re_h = Uh/\nu$ is usually quite small so that the effects of fluid inertia can be, and have been, ignored. However, the ratio $G/V = g'h^2/\nu U$ is typically quite large, $O(10^2)$, and the ratio $G/S = g'\rho h^2/\sigma$ of order one. Thus, in general, gravity cannot be ignored in determining the shape of the interface since it causes both an asymmetry in the flow field, in which $t_1 < t_2$ (figure 5), a down-slope, gravity-driven flow in the thin layers on the wall (see figure 1*a*), which results in a layer up to 10% thinner than that without such a flow and a bubble shape which must depend to some extent on gravity, away from the immediate vicinity of the bubble tip. In figure 11 (*a*) we attempt to give some indication of the various regions where each of these forces may be important without entering into a full-scale asymptotic analysis. In what follows we have not attempted to cover the complete range of these parameters but only that range which seemed important.

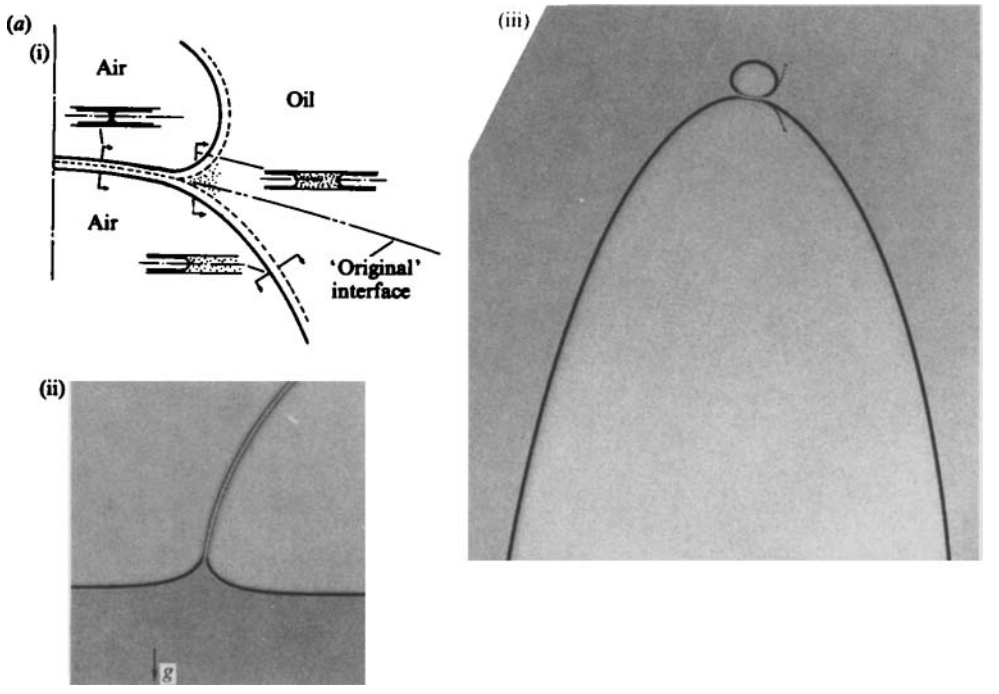

FIGURE 4(a). For caption see facing page.

However, for the simplest initial estimation, the velocity of rise of the bubble is calculated by assuming that local effects at the bubble edge are small and that the majority of the dissipation occurs in the outer flow, where the flow perpendicular to the plates is locally a plane Poiseuille flow while the mean streamlines, in the plane of the gap, are those of the potential flow caused by the bubble motion.

4.2. *The Taylor & Saffman (1959) and Tanveer (1986) theories*

Although the theory of bubble motion in a Hele-Shaw cell by TS is readily available in the open literature its interpretation in the present case is sufficiently subtle to warrant a relatively extensive re-examination. Although TS considered, in detail, the case of a bubble of width λW cm moving under the action of the pressure gradient generated by a uniform flow through a Hele-Shaw cell of width W cm, in the absence of surface-tension forces, it is appropriate here to consider immediately their brief extension to motion under the influence of gravity and a uniform upstream flow of velocity V. Here they defined a dependent parameter

$$U' = \frac{U - U^+}{V - U^+}, \tag{1}$$

where U is the bubble velocity and

$$U^+ = \frac{\mu_2}{\mu_1} U - \frac{h^2 g' \sin\alpha}{12\nu_1}.$$

Here $g' = g(\rho_1 - \rho_2)/\rho_1$; ρ_1 and μ_1 are the fluid density and viscosity and ρ_2 and μ_2 the bubble density and viscosity, while $\nu_1 = \mu_1/\rho_1$.

In our particular case $V = \mu_2 = \rho_2 = 0$ so that

$$U = -U^+(U' - 1) = \frac{h^2 g' \sin\alpha}{12\nu_1}(U' - 1). \tag{2}$$

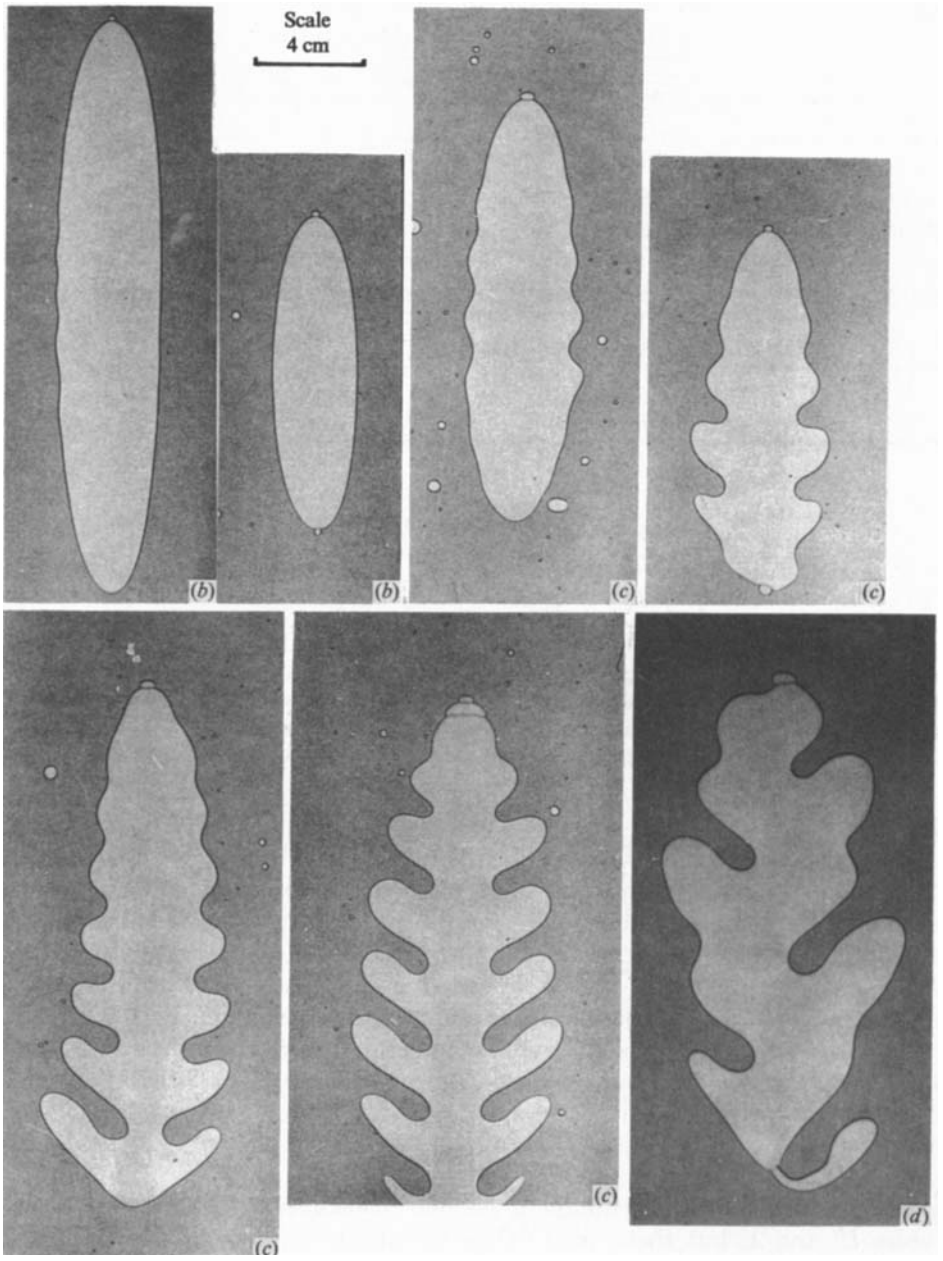

FIGURE 4. (*a*) Details of a the large bubble shapes and flow field at the nose of a large bubble to which a smaller bubble has become attached. (i) A sketch of the shape of the interface at which two bubbles meet showing the meniscus shapes at various locations and the thickness of the bridge between the two bubbles. The double-chain dotted line represents the shape of the undisturbed interface. (ii) Photograph of a rising bubble pair showing details of the intersection region, together with a superimposed drawing (dotted-line) of the static interface shown in (iii). (*b*) Examples of the change in shape created by a small bubble attached to the nose of a larger one. Without the attached bubble the larger would have an ellipticity of about 1.4 or would be unstable. (*c*) The wave produced by a large rapidly moving bubble with a smaller bubble at its leading front. (*d*) The asymmetric wave produced on a large bubble by the oscillation of a tip-bubble slightly larger than that shown in (*c*).

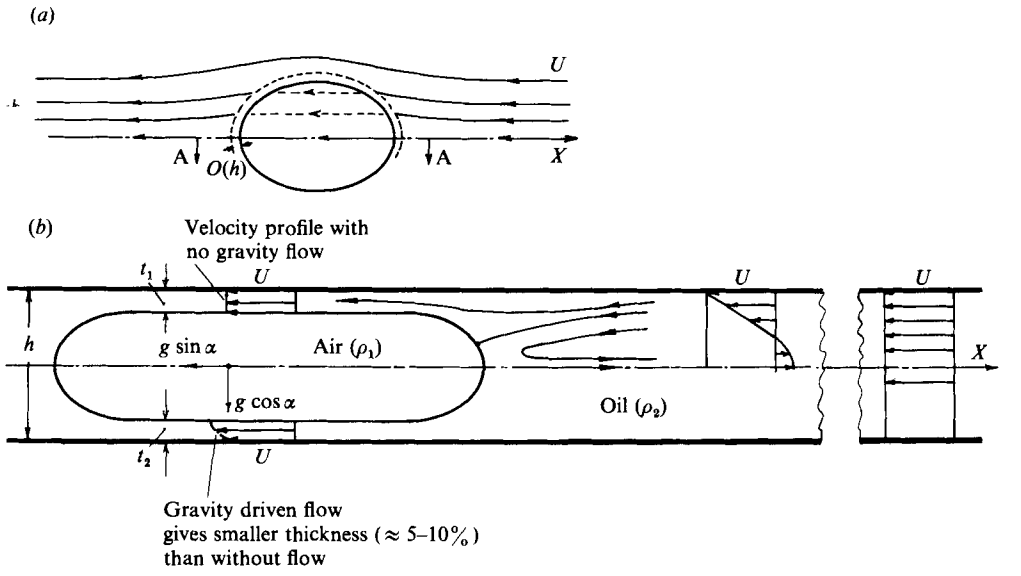

FIGURE 5. Flow field generated by the rise of a single bubble. (*a*) Mean outer flow streamlines in a bubble-centred frame of reference. Dotted interior streamlines indicate the mean flow, i.e. that averaged across the gap width. The region of thickness $O(h)$ is where the flow deviates from Poiseuille flow. (*b*) Cross-section at A–A. In this frame of reference the oil film between plate and bubble is moving with the wall velocity, U. Far upstream the flow is uniform, also with velocity U, and the recirculation bubble disappears. For lack of any better information we assume $t_1 = t_2$. To avoid confusing this figure, more information is given on figure 11 (*a*).

Furthermore, the ratio of the length of the bubble (L cm) to its width, λW(called D in what follows) is given by:

$$\frac{L}{D} = \frac{2}{\pi\lambda}\left(\frac{U'-1}{U'}\right)\tanh^{-1}\{\sin(\tfrac{1}{2}\pi U'\lambda)\}. \tag{3}$$

In the limit $\lambda \to 0$, i.e. a finite bubble in an infinitely wide cell, $(L/D)_{\lambda=0} = (U'-1)$ and the bubble is elliptical in shape, while the velocity of rise of this elliptical bubble, which we call U_e, is given by

$$U_e = \frac{h^2 g' \sin\alpha}{12\nu_1}\left(\frac{L}{D}\right)_{\lambda=0}. \tag{4}$$

Specifying the area of the bubble gives one relationship between the dependent variables U' and λ, but there then exists an infinite number of possible solutions corresponding to $1 < U' < \infty$ with no mechanism to choose between them.

TS then made the *ad hoc* speculation that at least one possible special solution could be found by minimizing the product $U'\lambda$, for fixed bubble area, since it 'may be identified intuitively with the rate at which fluid is pushed aside by the bubble'. This extremum in $U'\lambda$ occurs for the value $U' = 2$, in which case the bubble velocity is

$$U^* = \frac{h^2 g' \sin\alpha}{12\nu_1}, \tag{5}$$

and

$$\left(\frac{L}{D}\right)_{U'=2} = \frac{1}{\pi\lambda}\tanh^{-1}\{\sin(\pi\lambda)\}, \tag{6}$$

which represents just that bubble distortion required in order for the velocity to remain constant as the relative bubble width varies. Note that as $\lambda \to 0$ the bubble becomes circular in this case.

The further, detailed interpretation of these results is left until §6 where we discuss the experimental results. However, as we will see there these special results (5) and (6) are not sufficient to reduce the data since they only appear to be valid as $\alpha \to 0$. As a result, in our more general case, we are forced to use measured values of L/D in order to find the corresponding values of U' and hence U. Since this calculation involves the inversion of the transcendental equation (3) the result is not particularly convenient to use. After various trial-and-error calculations we have found that

$$\frac{(L/D)}{(L/D)_{U'=2}} \equiv \frac{2(U'-1)}{U'} \frac{\tanh^{-1}\{\sin(\frac{1}{2}\pi U'\lambda)\}}{\tanh^{-1}\{\sin(\pi\lambda)\}} \approx [U'-1], \tag{7}$$

to within 1–2 % over the ranges of λ and U' of interest. Thus the bubble velocity is given to a very good approximation by

$$U \approx \frac{h^2 g' \sin\alpha}{12\nu_1} \left(\frac{L}{D}\right) \left(\frac{D}{L}\right)_{U'=2}, \tag{8}$$

a result which appears to account for both the gravitationally induced elongation of the bubble and the proximity of the cell sidewalls.

The work of Tanveer (1986) was undertaken in an attempt to remove the non-uniqueness of the theory presented above by including the effect of finite, interfacial surface tension, cf. the work of McLean & Saffman (1981) in the corresponding problem of finger motion. An examination of his results makes it clear that he has been able to put the extremum principle of TS on a firmer footing, for indeed he finds that $U' \to 2$ as $\sigma \to 0$, in the notation of the present work. For values of $\sigma > 0$ he finds $U' < 2$, the actual values depending on the details of cell width, bubble area and fluid properties. We have interpolated within the tables of values he gives and have found the corrections to (6) resulting from the inclusion of σ for our cell geometry and fluid properties. These are plotted on figure 8 (*a*) together with the TS values (see (6)). The value of U' found in a similar way is still 2 to within 1–2 %, over our range of experimental parameters.

However, it appears that he has not found unique solutions which are able to explain the present experimental results for large values of α, since, as suggested by P. Saffman (private communication), he has not used the interfacial boundary conditions appropriate to the present problem and hence has not been able to find the values of $U' > 2$ which are needed in order to describe the experimental results.

4.3. *An alternative derivation for the velocity of rise of circular and elliptical bubbles in a wide cell*

Some of the results outlined above ((4) and (5)) can be found using an argument which makes the physical meaning of the equations a little more obvious and provides a basis for the further calculations of §6. We consider the bubble to be disk shaped, filling the gap between the plates (figure 6*a*). As it rises this bubble creates an unsteady flow field that has, at any given time, a potential flow in the mean-flow streamlines (ψ) given by

$$\psi = -\frac{U_*}{4} \frac{D^2}{r} \sin\theta, \tag{9}$$

where U_* is the velocity of rise, D the bubble width and r and θ cylindrical coordinates attached to the centre of the circle (figure 6*a*).

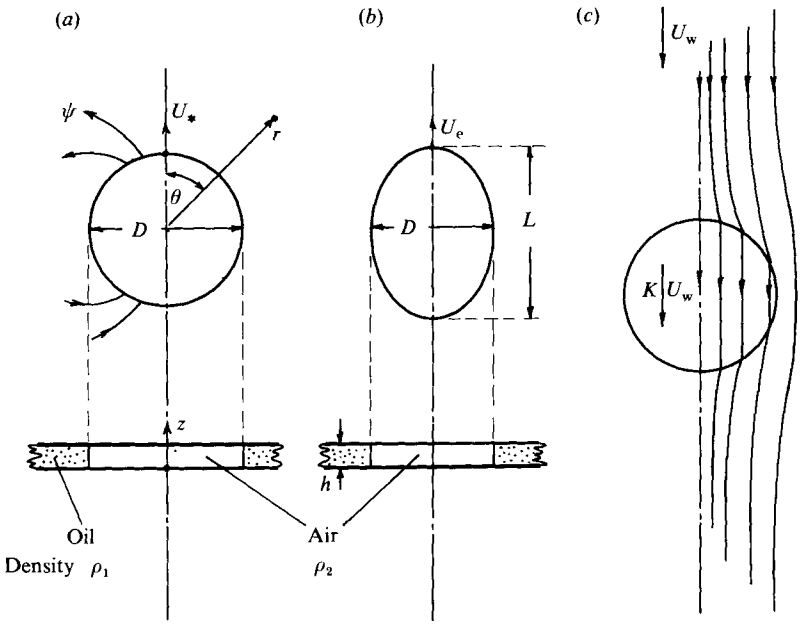

FIGURE 6. Model geometries. (*a*) Circular bubble (§4.3). (*b*) Elliptical bubble (§4.3). (*c*) Mean streamlines of the flow due to a bubble which does not fill the gap between the plates of the cell, in a frame of reference attached to the moving bubble (§6.1).

From (9) we see that the local mean velocity, i.e. the absolute value of the velocity averaged over the depth of the gap h is given by

$$\bar{U} = \frac{U_*}{4}\frac{D^2}{r^2}. \tag{10}$$

At each point (r, θ) the local velocity profile is that of plane Poiseuille flow so that the local dissipation is

$$\frac{12\mu_1 \bar{U}(r)}{h}\Big/\text{unit time/unit area}. \tag{11}$$

The total dissipation is, on substituting (10) into (11) and integrating over $\frac{1}{2}D \leqslant r \leqslant \infty$,

$$\frac{3\pi\mu_1 U_*^2 D^2}{h}\Big/\text{unit time}. \tag{12}$$

A similar calculation for an elliptical bubble (figure 6*b*) gives the same result, i.e. $3\pi\mu_1 U_e^2 D^2/h$.

In order to calculate U_* and U_e this total dissipation must be equated to the work done by the buoyancy force acting on the bubble

$$\left.\begin{aligned} &\tfrac{1}{4}\pi D^2 hg(\rho_1-\rho_2)\, U_* \sin\alpha \quad \text{for a circular bubble,} \\ \text{and}\quad &\tfrac{1}{4}\pi DL\, hg(\rho_1-\rho_2)\, U_e \sin\alpha \quad \text{for an elliptical bubble,} \end{aligned}\right\} \tag{13}$$

so that

$$U_* = \frac{g'h^2}{12\nu_1}\sin\alpha, \tag{14}$$

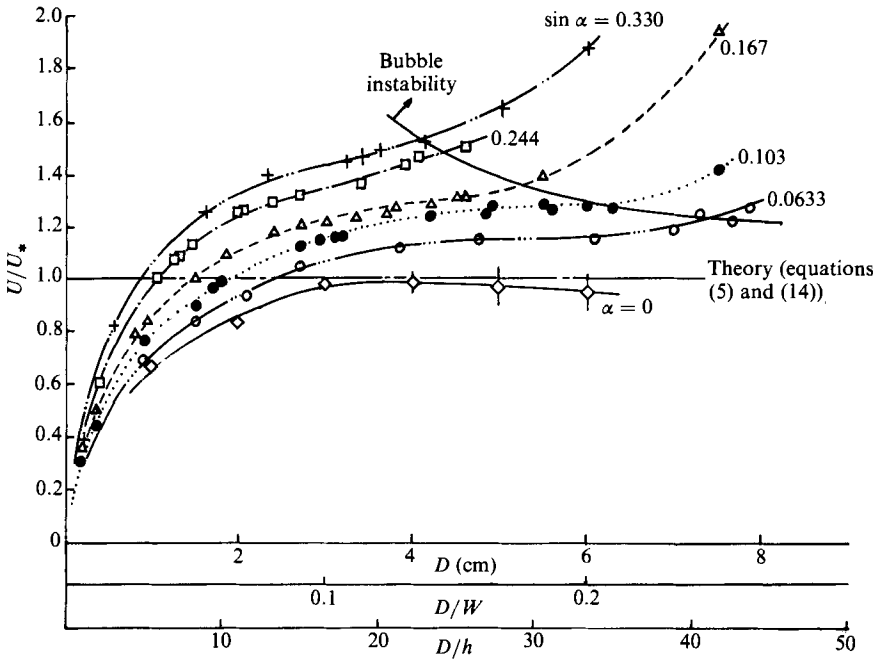

FIGURE 7. U/U_* *vs.* D, D/h and D/W for five values of α. The lower solid curve is the result of cross-plotting U/U_* *vs.* α for constant D and extrapolating to $\alpha = 0$. The solid horizontal line of $U/U_* = 1$ is the theoretical prediction for circular bubbles (equations (5) and (14)).

in the former case and

$$U_e = \frac{g'}{12}\left(\frac{L}{D}\right)\frac{h^2}{\nu_1}\sin\alpha, \tag{15}$$

in the latter, where $g' = g(\rho_1 - \rho_2)/\rho_1$ and α is the angle between the plane of the gap and the horizontal. These then agree with the TS results if we assume $U' = 2$, as obtained from their extremal hypothesis and Tanveer's numerical calculation.

The characteristic rise velocity, U_*, can then be used, initially, to reduce the raw data generated by the experimental procedure outlined in §2 and presented in §5. We do this because U_* is the only velocity scaling which uses the independent parameters of the problem and which does not force us to make *ad hoc* assumptions about the nature of the flow.

5. Results

Experiments were run over a range of values of α and bubble widths D and the resultant values of the bubble velocities and shape parameter, L/D, (see figure 6*b*) plotted in non-dimensional coordinates in figures 7 and 8. The actual shapes are shown in figure 9 for a few representative examples in order to show that the bubbles are close to being elliptical in shape. The observations that the curvature of the rear of the bubble is slightly larger than the front, under some circumstances, is similar to the plotted shapes of Tanveer (1986). As can be seen immediately from figure 7, the simplest theoretical result of TS (equation (5)) appears to be close to the lower limit of the experimental results for moderate bubble widths D only and for $\alpha \to 0$.

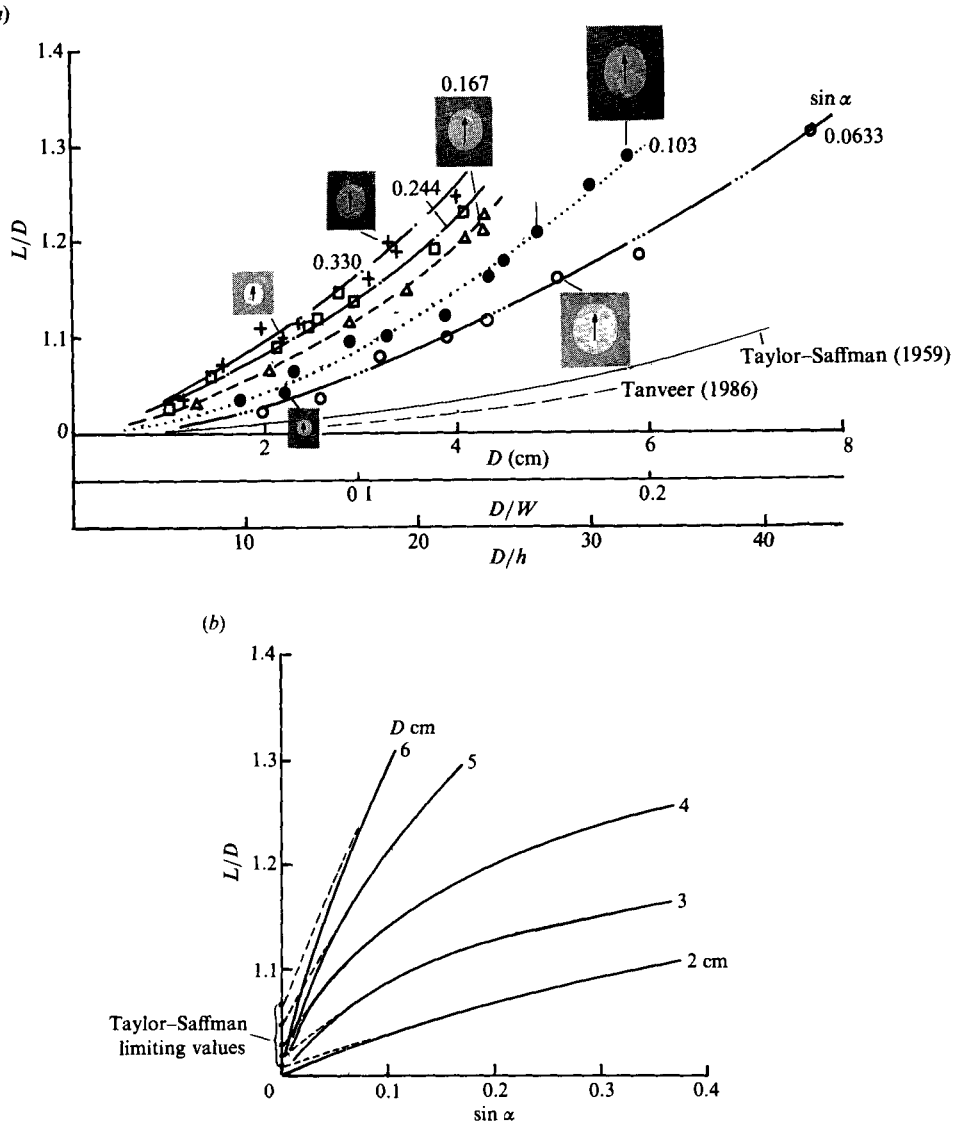

FIGURE 8. (*a*) Bubble shape parameter, i.e. bubble length (L)/bubble width (D) *vs.* D, D/h and D/W for various values of $\sin\alpha$. The TS values for their unique solutions ($U' = 2$) are shown, as are Tanveer's (1986) results for $\pi h^2\sigma/12W^2\mu = 3.1 \times 10^{-4}$. (*b*) L/D *vs.* $\sin\alpha$ for various values of D, with extrapolation to the TS values at $\alpha = 0$.

but that the actual bubbles have much higher velocities. It is clear also that the theory overestimates the bubble velocities for the smaller widths, having the wrong behaviour as $D \to 0$.

As anticipated in §4, the shape parameter (figure 8) gives some clue to the reason for the first of these observations since we see that for large D the bubble shape from TS is only approached as $\alpha \to 0$ and that the actual bubbles are far more elongated in the direction of their motion, thus resulting in a larger velocity (equations (4) and (8)). Above the line marked 'bubble instability' the bubbles underwent severe, unsteady distortions of shape, sometimes undergoing tip-splitting and rejoining and

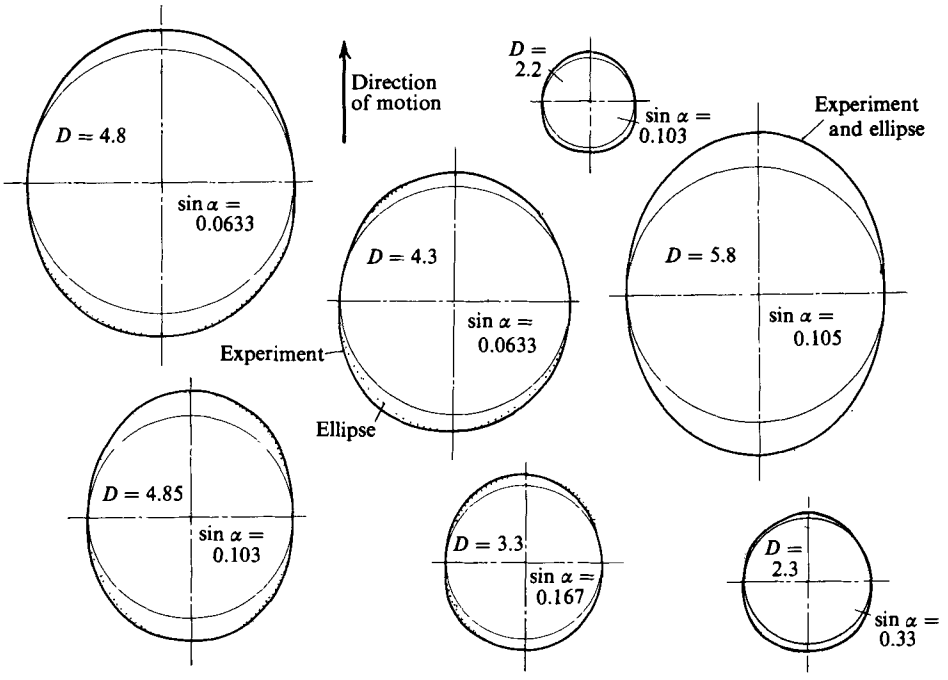

FIGURE 9. A selection of bubble planforms for values of the parameters shown on each figure. Here we see that while the assumption of an elliptical bubble is reasonable there are subtle differences. In particular, for the smaller bubbles the curvature of the leading surface is visibly greater than that of the trailing surface, an effect which may account for some of the small differences seen in figure 10. The photographic magnification is different for each bubble shape drawn here.

sometimes a periodic undulation in shape as in the related problem of finger propagation in a Hele-Shaw cell (Park & Homsy 1985; Maxworthy 1987; DeGregoria & Schwartz 1986). Also, in this case, the similarity to the stability of bubble flows in fluidized beds (Davidson & Harrison 1977) has not escaped our attention and deserves further study. However, all of these results are excluded from the discussion which follows and will be presented, in detail, in a future paper. Other reasons for the observed deviations are somewhat more subtle and are discussed in detail in §6.

6. Discussion

The results presented in the previous section seem to suggest that the special solutions found by TS and Tanveer (1986) only hold in the limit $\alpha \to 0$. This is a curious result because it appears to contradict the basic assumptions of both theories, since the effect of surface tension must dominate as α, and hence the bubble velocity, tends to zero. We hope that future experiments will clarify this result and determine if it is valid under very carefully controlled conditions.

In order to reduce these data further, it is necessary to examine the general results of TS and at least show that they are consistent with the experimental measurements. In order to do so we are forced to use one of the measured characteristics, e.g. L/D, in order to calculate the other, U (equation (8)). When we make this re-evaluation of the ordinate of figure 7, using (8), we find that although the results are closer to the theoretical value at moderately large values of D they are still 5–20% too high,

while at small values of D no improvement can be seen at all. The reasons for this are two-fold. At the larger values of D we have ignored the fact that the bubbles do not completely fill the gap between the plates so that the outer flow is, in reality, that caused by potential flow around a porous cylinder. For small values of D, major deviations from a plane Poiseuille flow occur in the neighbourhood of the bubble surface so that the enhanced dissipation there must account for the lower-than-predicted velocities found experimentally. In §§6.1 and 6.2 we examine each of these effects in turn and show that when they are included in the theoretical formulation they appear to reduce the difference between theory and experiment to an acceptable level in the one case and to explain the trends in the data satisfactorily in the other.

6.1. *Velocity of rise of a wetting bubble*

As shown in figure 5 and observed in all the experiments presented here, the flow in the neighbourhood of the bubble surface was quite complex. In particular, as it rose a thin film of oil was left between the plates and bubble interior. The thickness of this film depended on the bubble velocity but this dependence was not measured. The problem is similar to that presented previously by Fairbrother & Stubbs (1935), Bretherton (1961), Taylor (1961) and Reinelt & Saffman (1985) for bubbles moving through tubes and Park & Homsy (1984) and Reinelt & Saffman (1985) for a two-dimensional bubble. In particular, the numerical results of Reinelt & Saffman (1985) show excellent agreement with the experimental results for the film thickness left by a bubble forced through a horizontal tube for all values of the control parameter $U\mu/\sigma$, sometimes called the capillary number Ca. Their numerical results for two-dimensional bubbles also asymptote the previously determined result of Bretherton (1961), that the total film thickness k (i.e. the channel thickness minus the bubble thickness) is given by:

$$\frac{k}{h} = K \approx 1.337(Ca)^{\frac{2}{3}} \quad \text{for } Ca \lesssim 0.02. \tag{16}$$

For the same small values of Ca, i.e. ($\lesssim 0.02$) the axisymmetric case has the same asymptotic limit which we assume is valid in the present case also. Above $Ca \approx 0.02$ the axisymmetric and two-dimensional cases diverge slightly with the former having an asymptote at a value of $K \approx 0.67$ and the latter at a value of $K \approx 0.61$. However, of the range of present interest, i.e. $Ca < 0.1$ they are virtually identical.

In a frame of reference attached to the moving bubble the presence of the oil film results in a flow field which, in the mean, is identical to the potential flow around a porous, circular cylinder (figure 6*c*) inside which the mean velocity is KU.† This is, in fact, one of the problems first considered for study by Hele-Shaw in the cell named after him (Hele-Shaw & Hay 1901). This in turn results in an unsteady external flow given, at any instant, by

$$\psi = -U_{\mathrm{w}}(1-K)\frac{D^2}{4r}\sin\theta \tag{17}$$

cf. equation (9).

† Contrary to out assumption, it is likely that the film thickness is not uniform behind the curved leading surface. It has been proposed that it depends on the local normal velocity to the interface U_{N}, (such a result was found by Tabeling & Libchaber (1986) upon *assuming* that the thickness was zero when $U_{\mathrm{N}} = 0$; see also comments by McLean & Saffman (1981) on Pitts (1980)) that this cannot be completely correct can be deduced from our observation that the film thickness does not go to zero at the maximum cross-section of the bubble, at least for the relatively large values of Ca used here.

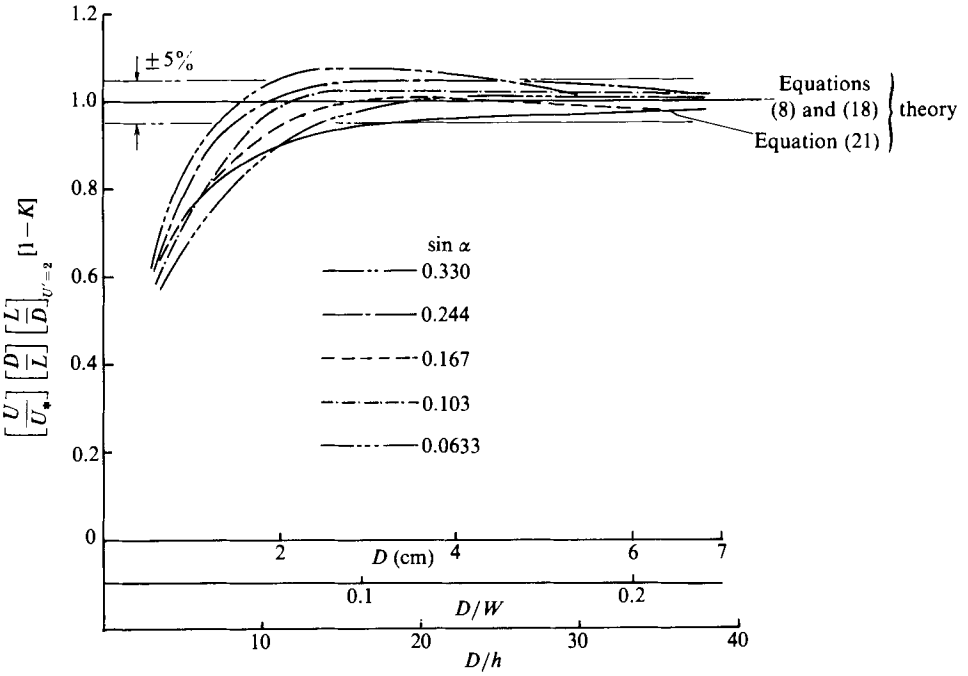

FIGURE 10. $[U(1-K)/U_*](D/L)(L/D)_{U'=2}$ *vs.* D/h and D/W for the raw data shown in figure 7.

As a result of the bubble rise velocity, U_w, becomes

$$U_w = \frac{g'h^2}{12\nu_1}\frac{\sin\alpha}{(1-K)}, \tag{18}$$

since the effective bubble volume, as in (13), must also be reduced by a factor of $(1-K)$. This result does not agree exactly with the formulation given in the appendix to Saffman & Taylor (1958) from which we would derive

$$U_w = \frac{g'h^2}{12\nu_1}\frac{(1-K^3)\sin\alpha}{(1-K)},$$

since we have ignored the small amount of dissipation which occurs in the thin films. However, the numerical results obtained from the two equations are negligibly different for the range of K of interest.

In the data reduction to compute the bubble velocity which follows we combine the effects due to ellipticity and wall effects (equation (8)) and wetting (equation (18)) using the measured values of (L/D), since we known of no numerical calculations of this quantity except Tanveer's (1986); and the numerical calculation of Reinelt & Saffman (1985) for K, but using the asymptotic results (equation (16)) for small values of Ca. The results of this re-non-dimensionalization of the experimental results are shown in figure 10 for values of bubble velocity below the line marked 'bubble instability' in figure 7. For consistency we have used the values of $(L/D)_{U'=2}$ from TS. Using the values from Tanveer (1986) (figure 8*a*) results in values which differ by at most 3% from those presented here for our particular cell geometry and fluid properties. Also, we have plotted the abscissa in two different ways: as D/h, since for small bubbles this appears to be the relevant parameter and as D/W since this seems more appropriate for large bubbles.

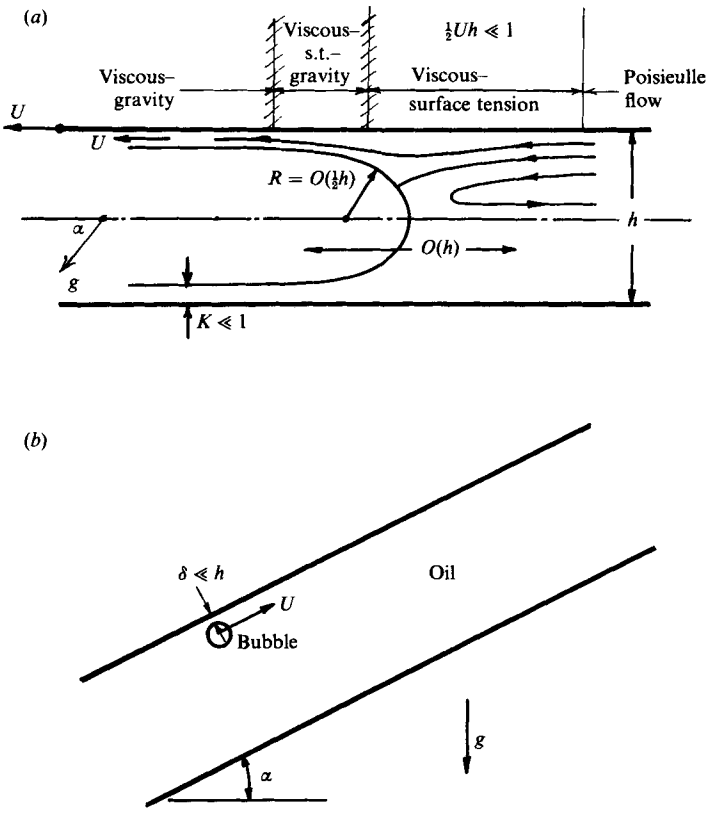

FIGURE 11. (*a*) Details of flow at the bubble surface showing the quantities discussed in §6.2, and the regions of force balance discussed in §4.1. (*b*) Bubble geometry for very small values of bubble diameter.

From figure 10 we see that the TS theory can be used to describe the experimental data in the range of bubble size $D/W \geqslant 0.07$ once the bubble shape is known, but that the downward trend at small values of D/h still needs explanation. The first statement implies that once the shape is known the interfacial boundary conditions no longer matter since the drag is then determined by the dissipation in the outer flow around the bubble, modified by the presence of the films and the sidewalls. We assume that small differences between curves are due to small effects which have not been modelled, e.g. that the bubbles are not perfectly symmetrical (figure 9); that the wetting film may not be of uniform thickness and is not stagnant under the action of gravity; that the various effects cannot be combined linearly, as assumed; etc.

6.2. *The velocity of rise for small values of D/h*

For small values of D/h we postulate that the enhanced dissipation at the bubble edge becomes important. Here the local pressure gradient can be estimated to be approximately

$$\left.\frac{\mathrm{d}p}{\mathrm{d}x}\right|_{\text{edge}} \approx \left(\frac{2\sigma}{h}\right)\frac{1}{h}, \tag{19}$$

i.e. we assume that the pressure difference across the bubble is developed in a distance

of order h and that $K \ll 1$ (figure 11*a*). The dissipation associated with this pressure gradient in the viscous flow is

$$\frac{C}{\mu}\left(\frac{\mathrm{d}p}{\mathrm{d}x}\right)_{\mathrm{e}}^2 h^3 2\pi D h = \frac{4\pi C D \sigma^2}{\mu} \tag{20}$$

on substitution from (19) and where C is constant (equal to $\frac{1}{12}$ for Poiseuille flow) i.e. we assume the flow remains similar as D changes. Thus the buoyancy work must balance both this dissipation plus that in the outer flow (equation (12)). On calculating the corrected U_{**} from this balance equation we find

$$\frac{U_{**}}{U_*} = \frac{1}{2} \pm \left\{\left(\frac{1}{2}\right)^2 - \frac{768 C \sigma^2}{h^4 (D/h)\,(g\Delta\rho)^2}\right\}^{\frac{1}{2}}. \tag{21}$$

This result is plotted in figure 10 for a value of $C = 0.003$ which makes the second term in the bracket equal to $0.036/(D/h)$ and gives good agreement with the experimental results for values of U_{**}/U_* not too different from unity. Based on this result it is possible, also, that the slight differences between the curves of figure 10 are due to variations in K which would result in a $\Delta\rho$ and hence C which depended on Ca.

While the details of the calculation given above are open to criticism the model shows, at least, that the details of the flow close to the bubble surface become more important as D/h decreases.

In the limit of very small bubble diameter the flow reduces to Stokes flow about a sphere close to a wall (figure 11*b*) which results in a bubble velocity approaching zero like D^2 as $D \to 0$ (Happel & Brenner 1973), a result which we cannot check in the present experiments.

I am grateful for discussions with Professors Saffman, Tanveer and Sadhal on the theory presented in §3 and for the comments of the referees. Casey de Vries constructed the apparatus with care. I wrote the preliminary manuscript while at the Department of Aeronautical Engineering, The Technion, Haifa, as Forman Visiting Professor in Aeronautics. I wish to thank Professors D. Weihs and M. Baruch for arranging this visit and providing such ideal conditions in which to work. The first version was expertly typed there by Mrs A. Goodman-Pinto and the final version by Mrs J. Givens at USC. Also, I wish to thank Professor G. K. Batchelor for inviting me to present this paper.

This work was supported by the ONR under Contract number N 00014-82-K-0084 to USC.

REFERENCES

Bretherton, F. P. 1961 The motion of long bubbles in a tube. *J. Fluid Mech.* **10**, 166–188.

Couder, Y., Cardoso, A., Dupuy, D., Tavernier, P. & Thom, W. 1986 Dendritic growth in the Saffman–Taylor experiment. *Europhys. Lett.* (to appear).

Davidson, J. F. & Harrison, D. 1977 *Fluidisation*. Academic.

DeGregoria, A. J. & Schwartz, L. W. 1986 A boundary-integral method for two phase displacements in Hele-Shaw cells. *J. Fluid Mech.* **164**, 383–400.

Fairbrother, F. & Stubbs, A. E. 1935 The bubble tube method of measurement. *J. Chem. Soc.* **1**, 527–529.

Happel, J. & Brenner, H. 1973 *Low Reynolds number hydrodynamics*. Leyden: Noordhof.

Hele-Shaw, H. S. & Hay, A. 1901 Lines of induction in a magnetic field. *Phil. Trans. R. Soc. Lond.* A **195**, 303–327.

LEVICH, B. G. 1962 *Physiochemical Hydrodynamics*. Prentice-Hall.

MCLEAN, J. W. & SAFFMAN, P. G. 1981 The effect of surface tension on the shape of fingers in a Hele-Shaw cell. *J. Fluid Mech.* **102**, 455–469.

MAXWORTHY, T. 1987 The non-linear growth of a gravitationally unstable interface in a Hele-Shaw cell. *J. Fluid Mech.* (in press).

PARK, C.-W. & HOMSY, G. M. 1984 Two-phase displacement in a Hele-Shaw cell. *J. Fluid Mech.* **139**, 291–308.

PARK, C.-W. & HOMSY, G. M. 1985 The instability of long fingers in a Hele-Shaw cell. *Phys. Fluids* **28**, 1583–1585.

PITTS, E. 1980 Penetration of fluid into a Hele–Shaw cell: the Saffman–Taylor experiment. *J. Fluid Mech.* **97**, 53–64.

REINELT, D. A. & SAFFMAN, P. G. 1985 The penetration of a finger into a viscous fluid in a channel and a tube. *SIAM. J. Sci. Stat. Comput.* **6**, 542–561.

RIEGELS, F. 1938 Zur Kritik des Hele-Shaw-Versuchs, *Z. angew. Math. Mech.* **18**, 95–106.

SHAW, R. 1984 *The Dripping Faucet as a Model Chaotic System*. Santa Cruz: Aerial.

SAFFMAN, P. G. & TAYLOR, G. I. 1958 The penetration of a fluid into a porous medium of Hele-Shaw cell containing a more viscous fluid. *Proc. R. Soc. Lond.* A **245**, 312–329.

TABELING, P. & LIBCHABER, A. 1986 Film draining and the Saffman–Taylor problem. *Phys. Rev.* A **33**, 794–796.

TANVEER, S. 1986 The effect of surface tension on the shape of a Hele-Shaw bubble. *Phys. Fluids* (submitted).

TAYLOR, G. I. 1961 Deposition of a viscous fluid on the wall of a tube. *J. Fluid Mech.* **10**, 161–165.

TAYLOR, G. I. & SAFFMAN, P. G. 1959 A note on the motion of bubbles in a Hele-Shaw cell and porous medium. *Q. J. Mech. Appl. Maths* **12**, 265–279.

TRYGGVASON, G. & AREF, H. 1983 Numerical experiments on Hele-Shaw flow with a sharp interface. *J. Fluid Mech.* **136**, 1–30.